

LASER APPLICATIONS IN BIOLOGY AND MEDICINE

PACS numbers: 87.85.fk; 73.21.Fg; 73.21.La; 78.60.Lc
DOI: 10.1070/QE2013v043n07ABEH014990

Simulation of a broadband nano-biosensor based on an onion-like quantum dot–quantum well structure

H. Absalan, A. SalmanOgli, R. Rostami

Abstract. **The fluorescence resonance energy transfer is studied between modified quantum-dots and quantum-wells used as a donor and an acceptor. Because of the unique properties of quantum dots, including diverse surface modification flexibility, bio-compatibility, high quantum yields and wide absorption, their use as nano-biosensors and bio-markers used in diagnosis of cancer is suggested. The fluorescence resonance energy transfer is simulated in a quantum dot–quantum well system, where the energy can flow from donor to acceptor. If the energy transfer can be either turned on or off by a specific interaction, such as interaction with any dyes, a molecular binding event or a cleavage reaction, a sensor can be designed (under assumption that the healthy cells have a known effect or unyielding effect on output parameters while cancerous cells, due to their pandemic optical properties, can impact the fluorescence resonance energy transfer parameters). The developed nano-biosensor can operate in a wide range of wavelengths (310–760 nm).**

Keywords: *quantum dot, quantum dot–quantum well structure, nano-biosensor, fluorescence resonance energy transfer.*

1. Introduction

Fluorescence resonance energy transfer (FRET) is a non-radiative mechanism due to which an excited-state donor transfers energy to a nearest ground-state acceptor through long-range dipole–dipole interactions [1–3]. One of the important parameters used in the FRET process is the rate of energy transfer which is highly dependent on many factors, such as spectral overlap between donor and acceptor, the relative orientation of the transition dipoles and the distance between the donor and acceptor molecules. FRET is very attractive for bio-analysis [4–6] because of its intrinsic sensitivity to nanoscale changes in donor/acceptor separation distance (proportional to r^6). The most significant application of FRET is biomarkers used in diagnosis of cancer if a set of molecular markers can be quantified and statistically differentiated between cancerous cells and healthy cells. It is well known that appropriate labelling of biological material and careful imaging provide a powerful tool for visualisation of the spatial distribution of cellular structures of interest.

H. Absalan, R. Rostami Department of Physics, Ahar Branch, Islamic Azad University, Ahar, Iran; e-mail: h-absalan@iau-ahar.ac.ir, r-rostami@iau-ahar.ac.ir;
A. SalmanOgli Photonics and Nanocrystal Research Laboratory, University of Tabriz, Tabriz, Iran; e-mail: araz.nano@gmail.com

Received 5 September 2012
Kvantovaya Elektronika **43** (7) 674–678 (2013)
Submitted in English

The exploitation of FRET can increase the spatial resolution of the fluorescence microscope to below 10 nm. This property is employed in FRET techniques ranging from the assay of interactions of an antigen with an antibody *in vitro* to the real-time imaging of protein folding *in vivo* [7–9]. In most cases, markers of diseases are often present at very low concentrations; therefore, the selected methods must be highly sensitivity and exhibit low detection limits. Quantum dots (QDs) [2, 10, 11] are nanoparticles that are attached to antibodies, aptamers, oligonucleotides, or peptides, thereby making them efficient target cancer markers. Fluorescent properties of QDs have enabled them to be used as labels for *in-vitro* assays to determine biomarkers; in addition, they have been investigated as in-vivo imaging agents [12–15]. The potential of multiplexed sensing using QDs with different emission wavelengths is promising for simultaneous detection of multiple biomarkers of disease. FRET also provides a nanoscale ruler: when donor and acceptor are attached to a biomolecule, the rate of FRET indicates the donor/acceptor distance. There has recently been a revival of interest in FRET in connection with single-molecule studies as a probe for conformations of biomolecules [15–17].

In this paper we show that a nano-biosensor [18–21] in the form of a quantum dot–quantum well system (QDQW; an onion-like heteronanocrystal) [22, 23], which is both a donor and an acceptor, can be designed by forming a path for energy flow followed by its turning on or off due to a molecular binding event or a cleavage reaction

2. Theory

FRET usually occurs when the overlap between the donor emission and the acceptor absorption is larger than 30%. The normal distance at which FRET is observed lies between 1 to 10 nm. The energy transfer efficiency $\mathcal{E}$, energy transfer rate K_r, Förster radius R_0 (the distance between the donor and acceptor at which the energy of the donor excitation with a probability of 50% decays due to energy transfer, while the other half with the same probability is wasted through other radiative or nonradiative channels such as heat transfer) and the degree of donor–acceptor spectral overlap $J(\lambda)$ are calculated by the formulas [24–28]:

$$\mathcal{E} = R_0^6/(R_0^6 + r^6) = 1 - \tau_{da}/\tau_d, \quad (1)$$

$$K_r = (1/\tau_d)(R_0/r)^6, \quad (2)$$

$$R_0 = 0.21[\kappa^2 n^{-4} Q_d J(\lambda)]^{1/6}, \quad (3)$$

$$J(\lambda) = \int_0^\infty f_d(\lambda)\varepsilon_a(\lambda)\lambda^4 d\lambda \left(\int_0^\infty f_d(\lambda) d\lambda \right)^{-1}, \quad (4)$$

where r is the donor–acceptor distance; τ_d and τ_{da} are the donor lifetimes with and without the acceptor presence taken into account; κ is the orientation factor ($0 < \kappa^2 < 4$); ε_a is the acceptor extinction coefficient (in $cm^{-1}\ M^{-1}$); f_d is the donor modified fluorescence intensity; λ is the wavelength; and n is the medium refractive index. The refractive index n for biomolecules in aqueous solutions is 1.4. The parameter $J(\lambda)$ is the degree of spectral overlap between the donor emission and the acceptor absorption. The values of $J(\lambda)$ and R_0 increase at higher acceptor extinction coefficients and greater overlap between the donor emission spectrum and the acceptor absorption spectrum.

The QDQW structure has been analysed by using the accurate 8-band K.P theory [29–31] (the K.P approximation is used to extract the diversity relation between semiconductor bonds, to study energy band properties and related wave-functions near the Γ point of the Brillouin zone) and the finite element method (FEM). In this work, we assumed that the QD surfaces modified and functionalised [32–34] and the prepared surface is used in simulations.

The K.P approximation finds widespread application in semiconductors and provides a method for calculating the amplitude u in the Bloch wave-function $\exp(i\boldsymbol{kr})u_n(\boldsymbol{r},\boldsymbol{k})$. The K.P theory allows one to calculate the band structure $E_n(k)$ near the band edge (Γ point). This theory can be applied to single or multiply degenerate bands to attach the material dispersion curve.

The time-independent Schrödinger equation for electrons has the form [29–32]:

$$H\psi = E\psi, \quad (5)$$

$$H = -\frac{\hbar^2}{2m^*}\nabla^2 + \frac{\hbar}{4m^{*2}c^2}(\nabla V \times \boldsymbol{p})\sigma + V(\boldsymbol{r}) - \frac{e^2 r}{\varepsilon_r} + l(l+1)\frac{\hbar^2}{2m^*}, \quad (6)$$

where H is the Hamiltonian; E are the energy eigenvalues; ψ are the electron wave-functions; $V(r)$ is the crystal potential; m^* is the electron–hole effective mass; $\hbar$ is Plank's constant; σ is the Pauli spin matrix; c is the speed of light; e is the electron charge; l is the orbital angular quantum number; ε_r is the dielectric constant of materials; and $\boldsymbol{p}$ the momentum operator. If we represent the sought for wave function of the form of a Bloch wave

$$\psi(\boldsymbol{r}) = \exp(i\boldsymbol{kr})u_n(\boldsymbol{r},\boldsymbol{k}), \quad (7)$$

then after the substitution of (7) in (6), we have

$$H = -\frac{\hbar^2}{2m^*}\nabla^2 + \frac{\hbar}{m^*}(\boldsymbol{kp}) + H_{per1} + H_{per2} + \frac{\hbar^2 k^2}{2m^*} + V(\boldsymbol{r}) - \frac{e^2 r}{e} + l(l+1)\frac{\hbar^2}{2m^*}. \quad (8)$$

Here, H_{per1} and H_{per2} are spin-orbit interaction operators of $\boldsymbol{k}$ dependent and $\boldsymbol{k}$ independent factors, respectively:

$$H_{per1} = \frac{\hbar}{4m^{*2}c^2}(\nabla V \times \boldsymbol{p})\sigma, \quad (9)$$

$$H_{per2} = \frac{\hbar}{4m^{*2}c^2}(\nabla V \times \boldsymbol{k})\sigma. \quad (10)$$

With account for periodic structure properties and distinguishing of $u_n(\boldsymbol{r},0)$, we can expand the basis of the periodic structure:

$$u_n(\boldsymbol{r},\boldsymbol{k}) = \sum_{m=1}^{N_{max}} C_m u_n(\boldsymbol{r},0), \quad (11)$$

where N_{max} is the number of bands that has been used for approximation of the semiconductor band structure near the Γ point. By substituting equation (11) into (10), we solve the problem for N_{max} discriminated and degenerated bands for the structure in question. In equation (10), the new Hamiltonian is used where u_n is replaced by the state with same energy and other wave-functions. We considered a crystal cell (8 electrons) rather than the whole crystal (~1023 electrons). Because for the basis of the solution use is made of $u_n(\boldsymbol{r},0)$, the $\boldsymbol{k}$-dependent perturbation has little effect on output and therefore we can neglect it in solving the original equation, which is very important. Rather than using the traditional method of 8-band K.P approximation (construction of $N_{max}\times N_{max}$ matrix), we utilised the FEM for solving N_{max} new Hamiltonian (modified by perturbation) equations. The final equation used for the solution by the FEM has the form

$$\sum_{m=1}^{N_{max}} \left[-\frac{\hbar^2}{2m^*}\nabla^2 + \frac{\hbar}{m^*}(\boldsymbol{kp}) + \frac{\hbar}{4m^{*2}c^2}(\nabla V \times \boldsymbol{p})\sigma + \frac{\hbar^2 k^2}{2m^*} + V(\boldsymbol{r}) - E(n,l) - \frac{e^2 r}{e} + l(l+1)\frac{\hbar^2}{2m^*} \right] u_n(\boldsymbol{r},\boldsymbol{k})C_m = 0. \quad (12)$$

3. Simulation, results and discussion

Different variants of the CdSe/ZnS/CdSe/ZnS physical structure and its potential profile are shown in Fig.1. The best method for covering a wide wavelength range (310–760 nm) is an alteration in the potential profile of the QD. Besides, other methods for covering the electromagnetic spectrum are employed, such as the alteration of the QD size and changing of the QD material composition, but they cannot span the full range of 450 nm. The composition of CdSe/ZnS/CdSe/ZnS is used in all in Fig. 1. These structures are found in diverse applications [22, 35, 36]. Their emission spectra are presented in Fig. 2. One can see that the luminescence spectrum of these structures overlaps the entire range in question.

Consider the FRET processes in a system consisting of two QDs, when the path is created for the energy flow from donor to acceptor. We assume that all particles (donors and acceptors) are excited by a conventional wideband source, and that the amount of acceptors and donors is 6×10^{16} (particle cm^{-3}). In this section, two examples of donor–acceptor interactions for St1 and St2 (Fig. 3) and St3 and St4 (Fig. 4) are investigated.

The 2-channel FRET between St1 as an acceptor and St2 as a donor is considered. In this process, the overlap between the donor emission and the acceptor absorption can reach $3.83\times10^{-21}\ cm^3\ M^{-1}$. An important parameter in the FRET

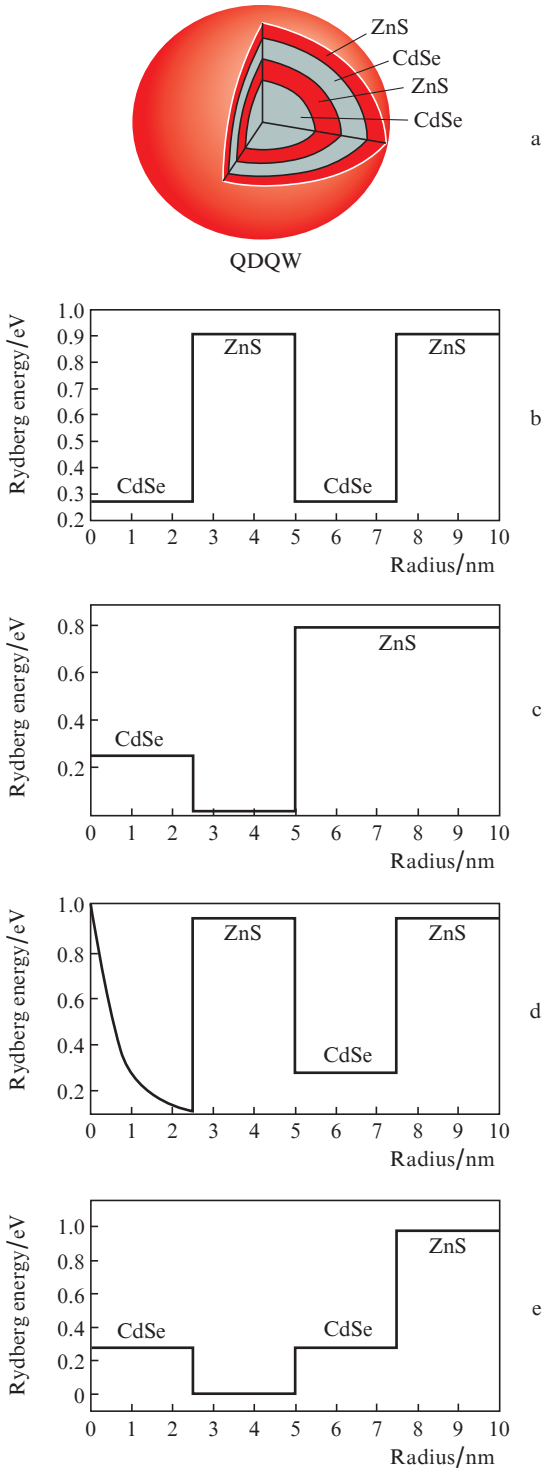

Figure 1. (a) QDQW schematic structure and potentials inside the onion-like QDQW heteronanocrystal (CdSe/ZnS/CdSe/ZnS) used in simulations of (b) St1, (c) St2, (d) St3 and (e) St4.

process is the donor lifetime to which the energy transfer rate is inversely proportional. For the donor lifetime of 1.56×10^{-6} s the rate of energy transfer from donor to acceptor(s) is very high (Fig. 3b). Moreover, the Förster radius alteration is described versus the quantum efficiency change (Fig. 3c). The maximum value of the radius is 0.73 nm. This 2-channel system can be regarded as a nano-biosensor, which should have high sensitivity to detect any disturbance such as entry of any dye molecules to the system.

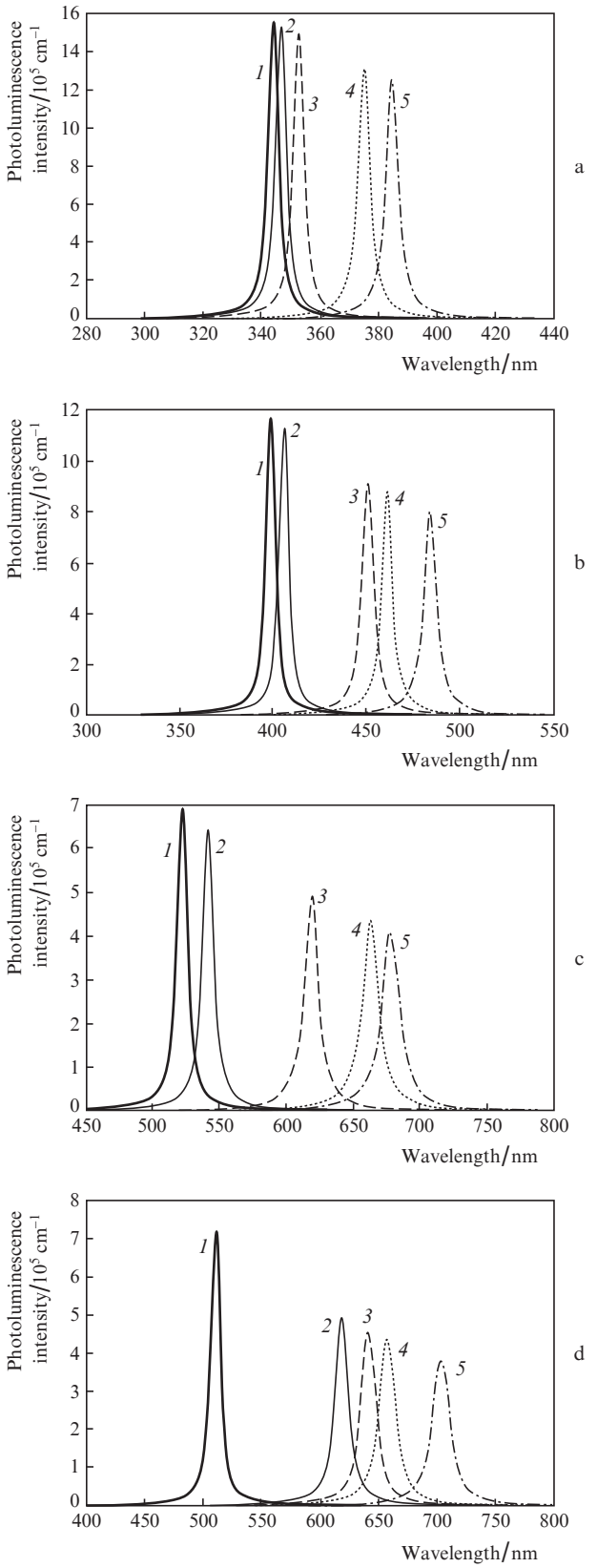

Figure 2. Photoluminescence intensity of structures (a) St1, (b) St2, (c) St3 and (d) St4 for different parameters [the QDQW radius is equal to (*1*) 4 and (*2–5*) 5 nm].

Note also that the donor lifetime must be higher than 50 ns because of existence of the auto-fluorescence and dye fluorescence. For this nano-biosensor to be used in other wavelength

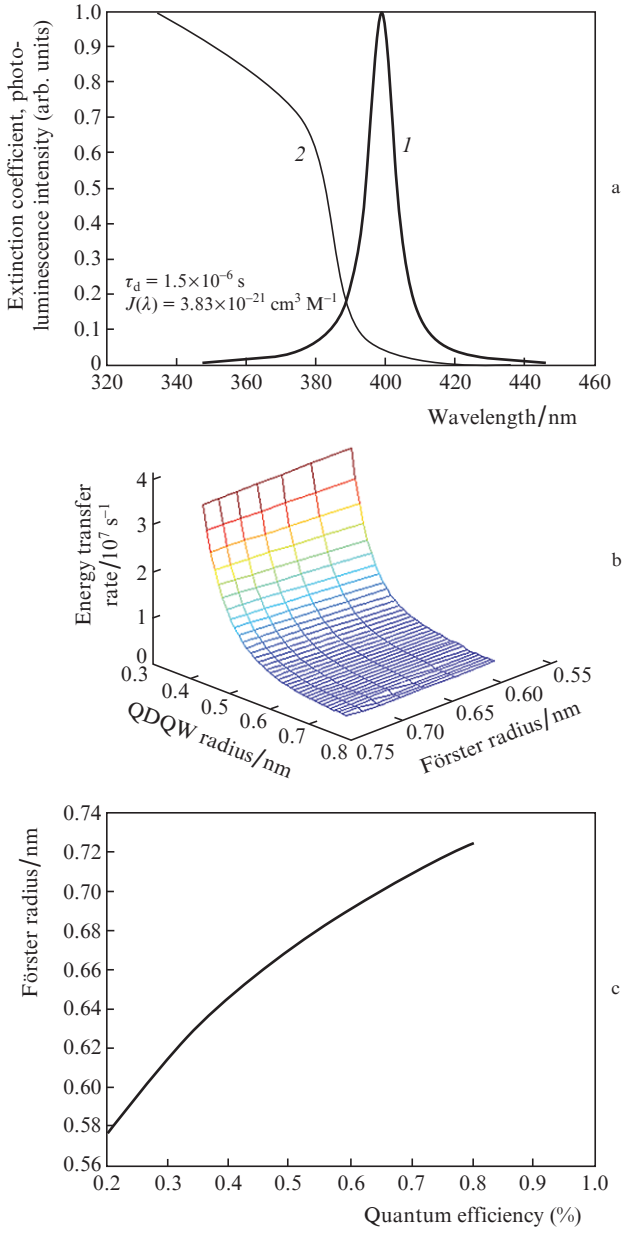

Figure 3. (*1*) Acceptor normalised extinction coefficient and (*2*) normalised photoluminescence intensity (a) as well as the energy transfer rate vs. radius of the QDQW system and Föster radius (b) and Föster radius vs. quantum efficiency (c) for the system consisting of St1 and St2.

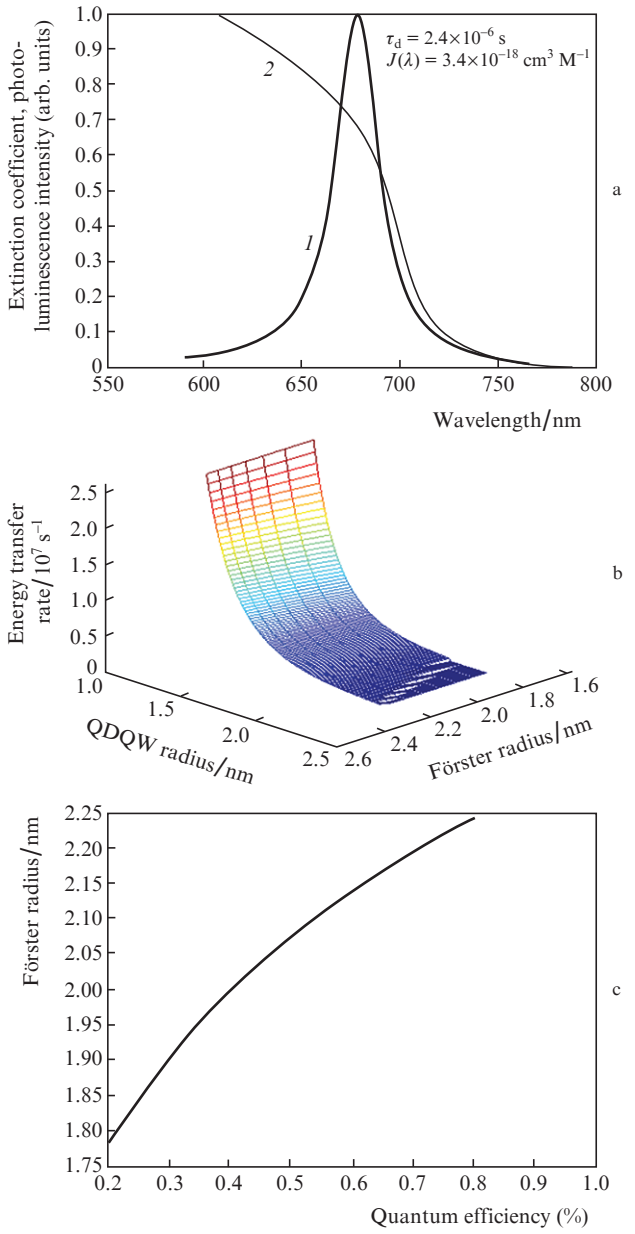

Figure 4. Same as in Fig. 3 but for the system consisting of St4 and St3.

ranges, we can consider another 2-channel system consisting of St3 and St4 (Fig. 4). In this case, the role of the acceptor is attributed to St4 and of the donor to St3. Then, the donor/acceptor overlap and the donor lifetime increase as compared to the previous case. Moreover, the Förster radius involves the range from 1.8 to 2.25 nm. The energy transfer rate is decreased to 2.5×10^8 s^{-1} due to increasing donor lifetime to 2.4×10^{-6} s.

Comparison of the above 2-channel FRET confirms that using differently designed nano-biosensors we can cover the considered wavelength range (310–760 nm). Besides other QD pairs can be introduced in which the overlap between the donor and the acceptor approaches zero (e.g., St1 and St3); therefore, the small disturbance or any dye molecule interactions in the considered range can be detected.

It is notable that the overlap between the donor (inorganic) and the acceptor (dye) is high due to the high molar extinction coefficient of the dye molecule in living organisms and due to its wide absorption spectrum. In this connection the designed nano-biosensor can play the role of a detector when any cancerous cells interact with the above-described 2-channel systems. Furthermore, such a sensor can help detect healthy cells and cancerous cells. Because the optical properties of cancerous cells (absorption and emission spectrum and molar extinction coefficients) differ from those of healthy cells, the applied disturbances of cancerous and healthy cells in the considered 2-channel systems are different. In order words, the defined pathway for transferring energy through donor to acceptor surely disrupts or turns off the entry of cancerous cells to systems, because the considered 2-channel system is converted to 3-channels, including two donors and one acceptor or two acceptors and one donor in which inorganic particles play the donor roles due to large lifetimes, wide absorption

bands, etc. and the attached molecule (dye) is an acceptor, since the traditional source cannot directly excite the dye molecule. Therefore, the designed broadband nano-biosensor can detect any unknown particles.

If C5-indocyanine dye is used as a dye molecule and St3 and St4 are regarded as donors (the maximum lifetime is 2.4×10^{-6} s), the values of the overlap are markedly increased because of the two donors' superposition, and approache 3.4×10^{-10} cm^3 M^{-1} (Fig. 5). Thus, the designed nano-biosensor can be treated as a highly sensitive biosensor, which is capable of detecting cancerous cells with high efficiency.

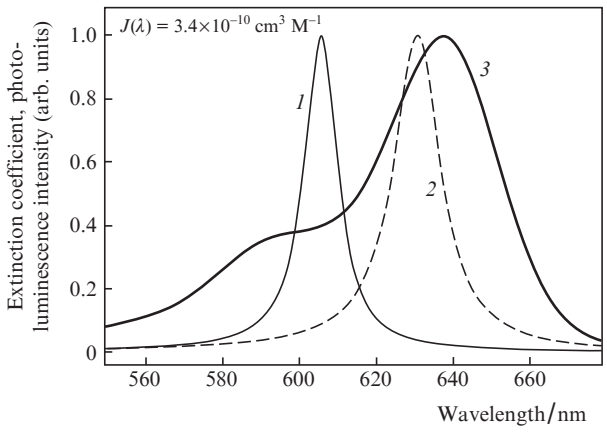

Figure 5. Emission spectra of QD (*1*) St3 ($\tau_d = 2.4\times10^{-6}$ s) and (*2*) St4 ($\tau_d = 2.2\times10^{-6}$ s) as well as the (*3*) absorption spectrum of CY5 dye molecule.

4. Conclusions

We have investigated the application of 2-channel FRET systems as nano-biosensors. The nano-biosensor designed can operate in a wide spectral range (310–760 nm) due to the alteration of the FRET parameters by manipulating the QDQW potential structure. It is shown that the control of the donor lifetime leads to a change in the Förster radii and improves the nano-biosensor parameters. Ultimately, the designed nano-biosensors have the ability to detect any disturbances of living organisms, including cancerous cells.

Acknowledgements. This work was supported by Ahar Branch, Islamic Azad University and Nano Ideh Pardazane ARAZ Co.

References

1. Zhong W. *Anal. Bioanal. Chem*., **394**, 47 (2009).
2. Sapsford K.E., Berti L., Medintz I.L. *Angew. Chem. Int. Ed*., **45**, 4562 (2006).
3. Frasco M.F., Chaniotakis N. *Sensors*, **9**, 7266 (2009).
4. Ho Y.P., Leong K.W. *Nanoscale*, **2**, 60 (2010).
5. Sapsford K.E., Pons T., Medintz I.L., Mattoussi H. *Sensors*, **6**, 925 (2006).
6. Wagner M.K., Li F., Li J., Li X.F., Le X.C. *Anal. Bioanal. Chem*., **397**, 3213 (2010).
7. SalmanOgli A. *Cancer Nanotechnol*., **2**, 1 (2011).
8. Dennis A.M., Bao G. *Nano Lett*., **8**, 1439 (2008).
9. Galvez E., Duser M., Borsch M., Wrachtrup J., Graber P. *Biochem. Soc. Trans*., **36**, 1017 (2008).
10. Kim S., Fisher B., Eisler H.J., Bawendi M. *J. Am. Chem. Soc*., **125**, 11466 (2003).
11. Brokmann X., Messin G., Desbiolles P., Giacobino E., Dahan M., Hermier J.P. *New J. Phys.*, **6**, 1 (2004).
12. Szafran B., Adamowski J., Bednarek S. *Physica E*, **5**, 185 (2000).
13. Absalan H., SalmanOgli A., Rostami R., Maleki S.A. *Adv. Sci. Eng. Med.*, **4**, 26 (2012).
14. Jare-Erijman E.A., Jovin T.M. *Nat. Nanotechnol.*, **21**, 1387 (2003).
15. Horvath G. *Ph.D. Thesis* (University of Deberecen, Medical and Health Science Center, Faculty of Science, 2005).
16. Cohen A.E., Mukamel Sh. *J. Phys. Chem. A*, **107**, 3633 (2003).
17. Rao J., Andrasi A., Yao H. *Curr. Opin. Biotechnol*., **18**, 17 (2007).
18. Algar W.R., Tavares A.J., Krull U.J. *Anal. Chim. Acta*, **673**, 1 (2010).
19. Willard D.M., Mutschler T., Yu M., Jung J., Van Orden A. *Anal. Bioanal. Chem*., **384**, 564 (2006).
20. Xing Y., Rao J. *Cancer Biomarkers*, **4**, 307 (2008).
21. Malicka J., Gryczynski I., Fang J., Lakowicz J.R. *Anal. Biochem.*, **317**, 136 (2003).
22. Nizamoglu S., Volkan H. *Opt. Express*, **16**, 3515 (2008).
23. SalmanOgli A., Rostami A. *J. Nanopart. Res*., **13**, 1197 (2010).
24. Saini S., Singh H., Bagchi B. *J. Chem. Sci*., **118**, 23 (2006).
25. Basko D.M., Granovich A.V.M., Bassani F., La Rocca G.C. *Eur. Phys. J. B*, **13**, 653 (2000).
26. Stricker S.J., Berg R.A. *J. Chem. Phys*., **3**, 814 (1962).
27. Roi B., Rabani E. *J. Chem. Phys*., **128**, 184710 (2008).
28. Zhangy L., Leng Y., Zhang J., Hu L. *J. Mater. Sci. Technol*., **26**, 921 (2010).
29. Enders P., Muller R., Klehr A., Gundlach H. *IEE Proc. Optoelectron*., **143**, 62 (1996).
30. Yoo H.K. *Ph.D. Thesis* (Texas Tech. University, 1971).
31. Geissbuhler I. *Ph.D. Thesis* (École Polytechnique Federale de Lausanne, 2005).
32. Mazumder S., Dey R., Mitra M.K., Mukherjee S., Das G.C. *J. Nanomater.*, **2009**, 815734 (2009).
33. Medintz I.L., Tetsuouyeda H., Goldman E., Mattoussi H. *Nat. Mater*., **4**, 435 (2005).
34. Nie S., Xing Y., Kim G.J., Simons J.W. *Annu. Rev. Biomed. Eng*., **9**, 257 (2007).
35. Rostami A., Rasooli H., Asghari Nrjad H.B. *Physica B*, **403**, 2789 (2008).
36. Rostami A., Rasooli H. *Microelectron. J*., **38**, 342 (2007).